In-flight calibration of the SWIFT XRT effective area

P. Romano[a], G. Cusumano[b], S. Campana[a], V. Mangano[b], A. Moretti[a], A.F. Abbey[c], L. Angelini[d], A. Beardmore[c], D.N. Burrows[e], M. Capalbi[f], G. Chincarini[a], O. Citterio[a], P. Giommi[f], M.R. Goad[c], O. Godet[c], G.D. Hartner[g], J.E. Hill[e], J. Kennea[e], V. LaParola[b], T. Mineo[b], D. Morris[e], J.A. Nousek[e], J. Osborne[c], K. Page[c], C. Pagani[a e], M. Perri[f], G. Tagliaferri[a], F. Tamburelli[f], A. Wells[c]

[a] INAF-Osservatorio Astronomico di Brera, Via Bianchi 46, 23807 Merate, LC, Italy
[b] INAF-IASF, Via U. La Malfa 153, 90146 Palermo, Italy
[c] University of Leicester, University Road, Leicester LE1 7RH, UK
[d] NASA-GSFC, Greenbelt, MD 20771, USA
[e] Pennsylvania State University, 525 Davey Lab, University Park, PA 16802, USA
[f] ASI-ASDC, Via G. Galilei, I-00044 Frascati, Italy
[g] Max-Planck-Institut für extraterrestrische Physik, Germany

ABSTRACT

The Swift X-ray Telescope (XRT) is designed to make astrometric, spectroscopic and photometric observations of the X-ray emission from Gamma-ray bursts and their afterglows in the 0.2-10 keV energy band. Here we report the initial results of the analysis of Swift XRT effective area as measured both on-axis and off-axis during the in-flight calibration phase using the laboratory results and ray-tracing simulations as a starting point. Our analysis includes the study of the effective area at a range of energies, for different event grade selection and operating modes using two astronomical sources characterized by different intrinsic spectra.

Keywords: Swift, XRT, Effective Area, Ancillary Response Files

1. INTRODUCTION

The Swift gamma-ray burst Explorer[1] was successfully launched on 2004 Nov 20. Its payload includes one wide-field instrument, the gamma-ray (15-350 keV) Burst Alert Telescope (BAT[2]) which detects the bursts, calculates their position to $\sim$ 1–4′ accuracy and triggers an autonomous slew of the observatory, and two narrow-field instruments, the X-Ray Telescope (XRT[3]), which operates in the 0.2–10 keV energy range and can provide $\sim 5''$ positions, and the Ultraviolet/Optical Telescope (UVOT[4]), which operates in the 1700–6000Å wavelength range and provides $\sim 0.5''$ positions.

The XRT is a focusing X-ray telescope that utilizes the third flight mirror module (FM3) developed for the JET–X program[5] and consists of 12 nested, cofocal and coaxial mirror shells arranged in a Wolter I configuration. The mirror diameters range from 191 mm to 300 mm and the focal length is 3.5 m, with a total field of view of $\sim$ 40 arcminutes (50% vignetting level, 1.5 keV). The XRT detector was designed for the EPIC MOS instruments on XMM–Newton and is a MAT-22 CCD consisting of 600 x 602 pixels (40μm $\times$40μm) with a plate scale of $2.36''$/pixel, which makes the effective field of view of the system $\sim 24'$.[6] The XRT Point Spread Function, as measured during the on-ground calibration, is $18''$ and $22''$ (HEW) at 1.5 keV and 8.1 keV, respectively. The XRT effective area is $\sim$135 cm^2 at 1.5 keV and $\sim$ 65 cm^2 at 8.1 keV, and depends on XRT read-out modes and grade selection. Four calibration sources are located at the corners of the detector to monitor the spectral resolution as the mission progresses.

XRT supports four different read-out modes to cover the dynamic range and rapid variability expected from GRB afterglows. The switch between modes is performed automatically[7] in order to minimize pile-up and optimize the collected information as the flux of the afterglow diminishes. In Imaging mode XRT produces an

Send correspondence to P. Romano, romano@merate.mi.astro.it, INAF-Osservatorio Astronomico di Brera, Via Bianchi 46, 23807 Merate, LC, Italy

integrated image (no X-ray event recognition takes place) which, for a typical GRB flux, is highly piled up. No spectroscopy is therefore possible, but a very accurate position and a good flux estimate can be obtained. The Photodiode mode (PD) is designed for very bright sources and for high timing resolution. Depending on the source count rate, two telemetry formats are available; at high fluxes (< 60 Crab) data are telemetred in Piled-up PD (PuPD) mode in which data are piled-up and spectral information is degraded; at lower fluxes (< 3 Crab) data are telemetred in Low Rate PD (LrPD) and full spectral information is available. The spectra of the four corner sources, however, are superimposed on the spectra of the astronomical sources (see Figure 1, left). High resolution light curves with a time resolution of 0.14 ms are generated. The Windowed Timing (WT) mode is obtained by binning and compressing 10 rows into a single row, and then reading out only the central 200 columns of the CCD (and effectively excludes the four calibration corner sources). It therefore covers the central 8 arcminutes of the field of view and provides one dimensional imaging and full spectral capability with a time resolution of 1.8 ms. This mode is used for fluxes in the range 1–600 mCrab. Finally, the Photon Counting mode (PC) allows full spatial and spectral resolution for source fluxes below 1 mCrab with a timing resolution of 2.5 seconds. X-ray events are classified according to the number and distribution of pixels in which they are detected, and are assigned 'grades' accordingly. While most of the X-rays from an astronomical source are expected to give raise to 1- or 2-pixel events (98% of the cases), the rest of events can cause 3- or 4-pixel events. To discriminate between them, XRT uses a library of grades which is derived from the XMM-Newton grading scheme. Default values of grades for astronomical sources are 0–5 for PuPD and LrPD, 0–2 for WT and 0–12 for PC mode.

The on-ground calibration of the XRT effective area was carried out in 2002 Sep 23–Oct 4 at the Panter laboratory of the Max-Planck-Institut für extraterrestrische Physik where the integrated system was tested.[8] Here we describe the early results of the in-flight calibration, in particular the latest Ancillary Response Files (ARF) generation and improvement, based on the spectroscopic study of several astronomical sources observed by XRT during the Calibration Phase, which ended on 2005 Apr 5.

2. THE METHOD

The XRT effective area is the product of three components: i) the effective area of the mirror, ii) the quantum efficiency (QE) of the CCD and iii) the filter transmission. In the specific case of XRT, the QE is included in the redistribution matrix (RMF) while the ARFs include the mirror effective area and filter transmission, as well as the vignetting correction and the Point Spread Function (PSF) correction, as a function of the source location and of the size of the extraction region. The RMFs and the PSF corrections are described in detail in accompaning papers.[9,10] Here we report on the method we used to generate the ARF files (distributed through CALDB) which represent the effective area of the telescope for a nominal on-axis observation (no vignetting correction) and for an infinite region of interest (no correction for PSF losses)*. We generated ARFs for PC, WT and LrPD XRT modes, and for different grade selections for each mode†, as an improvement upon the on-ground ones.

In general, there are two different methods of improving the instrument ancillary files starting from the on-ground ARFs. The first (microscopic) one relies on the knowledge of the physical processes related to the X-ray photon detection and aims at refining the physical parameters (e.g. gold density, inclusion of a carbon layer, CCD depletion depth, etc). The ARFs thus produced are then tested against well-known astrophysical sources to fine-tune the physical parameters. The second (macroscopic) method relies on our knowledge the spectra of well-known, stable astrophysical sources from previous X-ray missions. The on-ground ARFs are modified so that the resulting XRT spectrum becomes consistent with the observed ones through detailed modeling of the residuals.

Our choice of astrophysical sources for in-flight calibration of the ARFs fell on Crab-like supernova remnants (plerions), which are sources characterized by well known and stable power law spectral distributions. In par-

*To produce the observation-specific ARF files, the xrtmkarf task (HEASDAS software) has been developed, which corrects the nominal ARF file for the vignetting and, optionally, for PSF losses.

†The adopted calibration method implies that in the CALDB ARF files we include the residual correction of the CCD quantum efficiency. This explains why the nominal ARF files are different for different grade selections.

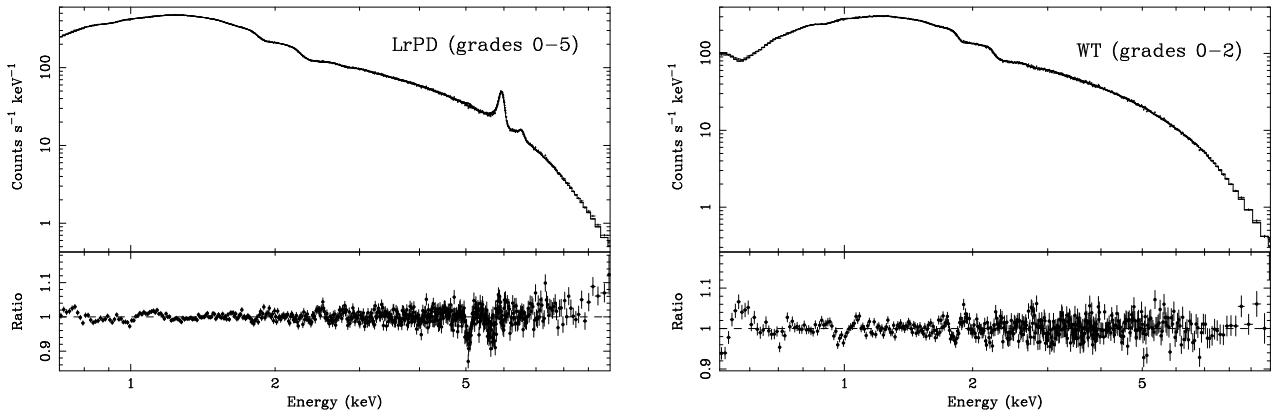

Figure 1. Left: Spectrum of the Crab in LrPD mode (grades 0-5) with the best fit model and the data/model ratio. Note that while the lines at 5.9 and 6.5 keV are due to the on-board calibration sources, the aborption feature at 5 keV is due to residual calibration uncertainties. Right: Spectrum of the Crab in WT mode (grades 0-2) with the best fit model and their ratio.

ticular, the XRT effective area was calibrated using the Crab nebula (for LrPD and WT modes) and the 50 ms pulsar PSR B0540-69 and its plerion (PC mode).

3. DATA PROCESSING AND RESULTS

The XRT data were first processed by the Swift Data Center at NASA/GSFC into Level 1 products (calibrated and quality-flagged event lists). Then they were further processed with the XRTDAS (v1.2 for LrPd and WT; v1.4 for PC mode) software package written by the Agenzia Spaziale Italiana (ASI) Science Data Center and distributed within FTOOLS v6.0 to produce the final cleaned event lists. Only observing time intervals with a CCD temperature below −47 Celsius were used. Further non-standard selections were performed to remove time intervals with high background rate caused by either dark current or by the bright Earth limb. Hot and flickering pixels were also removed. We used the latest RMF matrices (v007).

3.1. On-Axis Ancillary Response Files

3.1.1. LrPD Mode

To calibrate the LrPD ancillary files we considered an on-axis 6742 s exposure of the Crab, resulting in 5.5×10^6 counts (0.5–10 keV). The high absorption at low energies did not allow us to calibrate the spectrum below 0.5 keV. A procedure of ARF optimization was applied to the LrPD ancillary files generated from on-ground calibrations. We thus produced a final LrPD ARF file that, applied to Crab data, will reproduce its spectral energy distribution with best fit parameters consistent with those reported in the literature and based on data collected by other satellites (BeppoSAX[11] and RXTE[12]). As an example, in Figure 1 (left) we show the spectrum of the Crab nebula in LrPD mode (grades 0-5) obtained after correcting the ARF file, as well as the best fit model (an absorbed power law) and the data/model ratio. The reduced $\chi^2_{\rm red}$ is 1.5 (919 degrees of freedom, dof). We estimate a systematic uncertainty at the 5% level for all (i.e. different grade selections) LrPD ARF matrices in the 0.5-10 keV energy range. We note that while the lines at 5.9 and 6.5 keV are due to the on-board calibration sources, the absorption feature at 5 keV and an excess above 8 keV are due to residual calibration errors. Table 1 summarizes the fit results and shows how the fit values derived with the newly created ARF files are consistent with the ones from BeppoSAX fits.

3.1.2. WT Mode

To calibrate the WT ARFs we used an on-axis 4373 s observation of the Crab, that yielded 2.2×10^6 counts in the energy range 0.5-10.0 keV. Differently from LrPD, the WT data were affected by moderate pile-up. To

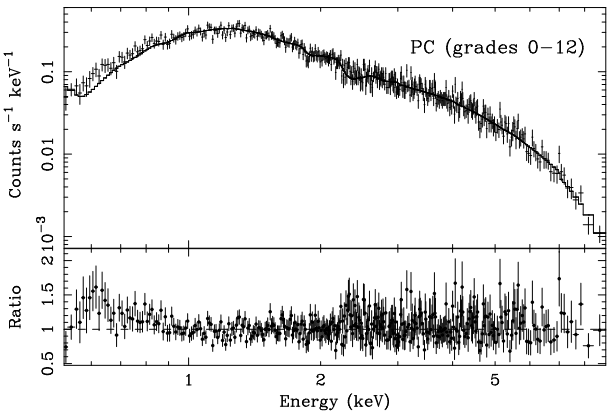

Figure 2. Spectrum of PSR B0540-69 in PC mode (grades 0–12, upper panel) together with the best fit model and the data/model ratio (lower panel).

correct for it, we extracted the off-pulse Crab spectrum by applying a phase-resolved analysis and verified that in this case the pile-up is negligible. We modified the on-ground WT ancillary files to reproduce the nebular spectral model parameters reported in the literature. Figure 1 (right) shows the residuals obtained by fitting the phase-resolved Crab nebula spectrum with an absorbed power law. The fit yields $\chi^2_{\rm red} = 1.4$ (943 dof). We estimate a systematic uncertainty at a level of 5% for all grades and in the 0.5-10 keV energy range. The strongest remaining features in the spectrum due to calibration errors are an emission line at ~ 0.6 keV and an absorption feature at ~ 1 keV. Table 1 shows how our fit values are consistent with the ones from BeppoSAX fits.

3.1.3. PC Mode

PC mode ARFs were calibrated with the Crab-like plerion PSR B0540-69 since the Crab spectra were unacceptably piled-up. The source has a count rate of ~ 0.7 counts s^{-1} but due to its moderate nebular extension (10–15″) it does not suffer from significant pile-up. The ARF optimization was performed on a 32 ks exposure that yielded 22400 counts (0.2–10 keV). The PSR B0540-69 best fit parameters are reported in the literature based on previous X-ray missions (BeppoSAX/MECS and XMM-Newton, see Table 1). Figure 2 shows spectrum, best fit model and the data/model ratio ($\chi^2 = 1.3$ for 130 dof, see Table 1). The statistical uncertainty on the final ARF matrices in PC mode is higher than for the other modes and is estimated at the 10% level in the 0.5-10 keV energy range. A strong and broad emission feature is present at ~ 0.6 keV. Table 1 shows how our fit values are consistent with the ones from both BeppoSAX and XMM-Newton fits.

Table 1. Best fit parameters for the Crab and PSR B0540-69 nebulae. The quoted errors are at 90% confidence level for one interesting parameter.

Target	Observatory	$N_{\rm H}$ (10^{22} cm^{-2})	Photon Index	Normalization	$\chi^2_{\rm red}$ (dof)
Crab	SAX/MECS	0.36 ± 0.02	2.09 ± 0.01	9.67 ± 0.01	1.7 (175)
	Swift/XRT/LrPD	0.35 ± 0.01	2.12 ± 0.01	9.86 ± 0.02	1.8 (939)
	Swift/XRT/WT	0.36 ± 0.01	2.10 ± 0.01	9.71 ± 0.03	1.4 (943)
PSR B0540-69	SAX/MECS	0.38 (fixed)	1.95 ± 0.02	0.0110 ± 0.0003	1.1 (89)
	XMM/MOS1	0.380 ± 0.002	1.96 ± 0.01	0.0102 ± 0.0003	1.2 (649)
	XMM/PN	0.410 ± 0.002	2.15 ± 0.02	0.0122 ± 0.0003	1.2 (1958)
	Swift/XRT/PC	0.35 ± 0.01	1.95 ± 0.01	0.0099 ± 0.0003	1.5 (474)

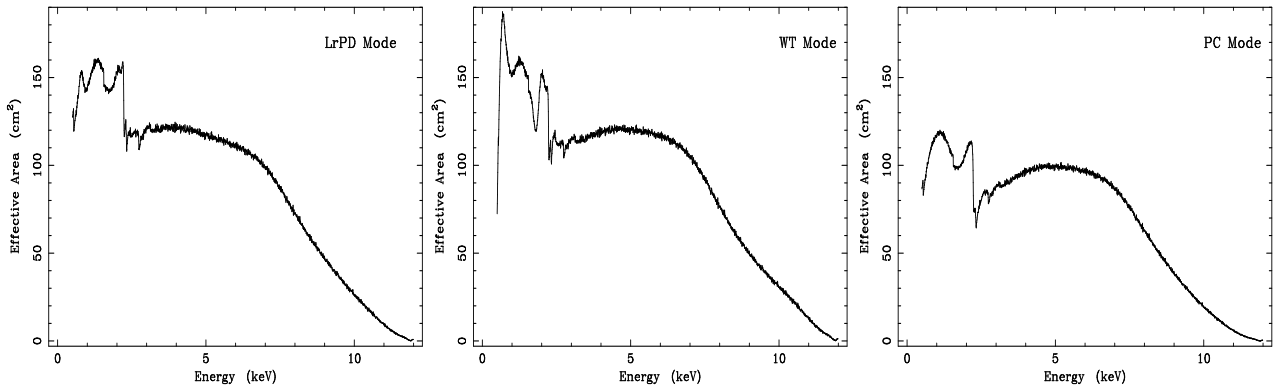

Figure 3. On-axis effective areas for different modes, LrPD (grades 0-5; left), WT (grades 0-2; center), and PC (grades 0-12; right).

Figure 3 shows our on-axis effective areas for the different observing modes, LrPD (grades 0-5; left), WT (grades 0-2; center), and PC (grades 0-12; right).

3.2. Off-axis: Correction for Vignetting

The XRT mirrors suffer from a reduction of the off-axis collecting area which is not taken into account in the distributed ARF files. We can however quantify the correction for vignetting by defining a vignetting function $V(\theta)$,

$$V(\theta) = 1 - C\theta^2 \tag{1}$$

where θ is the off-axis angle, and the coefficient C is a function of energy (in keV),

$$C(E) = P_0 \times E^{P_1} + P_2 \tag{2}$$

where P_0, P_1 and P_2 are parameters to be confirmed observationally. The XRT vignetting parameters we first measured during the on-ground calibration[8] and are now being tested by fitting Crab data observed at different off-axis pointings from $1.9'$ up to $7.5'$ off-axis angles. The best fit parameter values (absorbing column $N_{\rm H}$, photon index Γ and 0.2–10 keV flux) as a function of θ are reported in Table 2, and illustrated in Figure 4. The best-fit values of $N_{\rm H}$ are shown to vary by 0.3–10%, Γ by 0.3–4% and the flux by 0.7–10% (the higher value is for $\theta = 4.9'$).

Table 2. Crab nebula best fit parameters at different off-axis angles. The quoted errors are at 90% confidence level for one interesting parameter.

θ ($'$)	$N_{\rm H}$ (10^{22} cm^{-2})	Photon Index	0.2–10 keV Flux (10^{-8} ergs keV^{-1} sec^{-1})	$\chi^2_{\rm red}$ (dof)
1.9	0.360 ± 0.002	2.099 ± 0.002	5.89 ± 0.02	1.7 (939)
2.9	0.361 ± 0.002	2.105 ± 0.004	5.85 ± 0.03	1.1 (662)
4.9	0.397 ± 0.010	2.190 ± 0.020	6.36 ± 0.10	1.1 (334)
5.8	0.354 ± 0.002	2.074 ± 0.005	5.32 ± 0.04	1.1 (627)
7.5	0.384 ± 0.007	2.140 ± 0.010	6.16 ± 0.10	1.0 (325)

4. INTER-CALIBRATION WITH XMM-NEWTON AND BEPPOSAX

An initial approach to inter-calibration with other observatories was performed between XRT and XMM-Newton and BeppoSAX using PSR B0540-69 as a standard candle. We retrieved archival data obtained with the

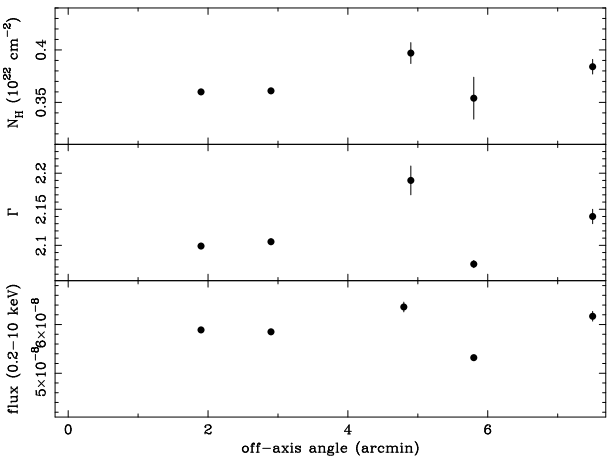

Figure 4. Variation of the best fit parameters with the off-axis angle for the Crab.

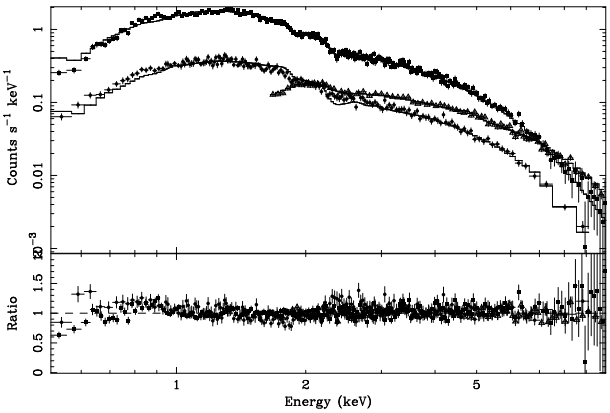

Figure 5. Initial intercalibration of XRT (circles), XMM-Newton/MOS (squares) and BeppoSAX/MECS (triangles).

XMM/MOS1 and BeppoSAX/MECS on 2001 May 23 and 1996 Oct 25, respectively. The net exposures were 22484 s with MOS1 (70936 counts) and 47845 s with MECS (25138 counts). We performed a simultaneous fit using an absorbed power-law model and allowing for the relative normalizations to vary. Figure 5 shows the spectrum of PSR B0540-69 for XRT (PC mode, grades 0–4), XMM/MOS1 and BeppoSAX/MECS, together with the best fit model (upper panel) and the data/model ratio (lower panel). The normalization factors indicate that XRT fluxes are within 2% of the MOS and 5-6% of the MECS.

These values are consistent with current work[13] based on the analysis of the afterglow of GRB 050326, which indicates that XRT/PC and XMM/EPIC/MOS1/MOS2/PN are calibrated in flux to within 3-8%. This is further confirmed by an analysis of the Crab data obtained with most modern observatories.[14]

5. CONCLUSIONS AND FUTURE WORK

The in-flight calibrations demonstrate that the effective area satisfies the mission requirements, since the statistical uncertainty on the on-axis ARF matrices we created range from the 5% level in LrPD and WT modes (0.5-10 keV) to 10% level in PC mode (0.5-10 keV). Further improvement of the ARFs, especially at the low energy end of the spectrum, will come from the application of our method to soft sources, such as the isolated neutron stars RXJ1856.4-3754 (for WT and PC) and RXJ0720.4-3125 (for PC). The cross-calibration of XRT and XMM-Newton will also benefit from an analysis of archival XMM-Newton data on the stable source PSR

B0540-69 and from a cross-calibration campaign with XMM on the active galactic nuclei H1426+428 (2005 Jun, to refine the PC ARFs) and 3C273 (2005 Jul, for WT) that is being performed during Summer 2005. As far as the off-axis correction is concerned, the analysis of the data which will be collected as part of the on-going in-flight calibration time allocation will improve our determination of the vignetting parameters P_0, P_1 and P_2 with respect to the on-ground-determined ones.[8]

ACKNOWLEDGMENTS

This work is supported at OAB by ASI grant I/R/039/04, at Penn State by NASA contract NAS5-00136 and at the University of Leicester by PPARC of grants PPA/G/S/00524 and PPA/Z/S/2003/00507. We gratefully acknowledge the contributions of dozens of members of the XRT team at OAB, PSU, UL, GSFC, ASDC, and MSSL and our subcontractors, who helped make this instrument possible.

REFERENCES

1. N. Gehrels, G. Chincarini, P. Giommi, K. O. Mason, J. A. Nousek, A. A. Wells, N. E. White, S. D. Barthelmy, D. N. Burrows, L. R. Cominsky, K. C. Hurley, F. E. Marshall, P. Mészáros, P. W. A. Roming, L. Angelini, L. M. Barbier, T. Belloni, S. Campana, P. A. Caraveo, M. M. Chester, O. Citterio, T. L. Cline, M. S. Cropper, J. R. Cummings, A. J. Dean, E. D. Feigelson, E. E. Fenimore, D. A. Frail, A. S. Fruchter, G. P. Garmire, K. Gendreau, G. Ghisellini, J. Greiner, J. E. Hill, S. D. Hunsberger, H. A. Krimm, S. R. Kulkarni, P. Kumar, F. Lebrun, N. M. Lloyd-Ronning, C. B. Markwardt, B. J. Mattson, R. F. Mushotzky, J. P. Norris, J. Osborne, B. Paczynski, D. M. Palmer, H.-S. Park, A. M. Parsons, J. Paul, M. J. Rees, C. S. Reynolds, J. E. Rhoads, T. P. Sasseen, B. E. Schaefer, A. T. Short, A. P. Smale, I. A. Smith, L. Stella, G. Tagliaferri, T. Takahashi, M. Tashiro, L. K. Townsley, J. Tueller, M. J. L. Turner, M. Vietri, W. Voges, M. J. Ward, R. Willingale, F. M. Zerbi, and W. W. Zhang, "The Swift Gamma-Ray Burst Mission," *The Astrophysical Journal* **611**, pp. 1005–1020, 2004.
2. S. D. Barthelmy and et al., "Burst Alert Telescope (BAT) on the Swift MIDEX mission," *Space Science Review* **120**, p. in press, 2005.
3. D. N. Burrows and et al., "The Swift X-Ray Telescope," *Space Science Review* **120**, p. in press, 2005.
4. P. W. Roming and et al., "The Swift Ultra-Violet/Optical telescope," *Space Science Review* **120**, p. in press, 2005.
5. O. Citterio, S. Campano, P. Conconi, M. Ghigo, F. Mazzoleni, E. Poretti, G. Conti, G. Cusumano, B. Sacco, H. Brauninger, W. Burkert, R. Egger, C. M. Castelli, and R. Willingale, "Characteristics of the flight model optics for the JET-X telescope onboard the Spectrum-X-Gamma satellite," *Proc. SPIE* **2805**, pp. 56–65, 1996.
6. D. N. Burrows, J. E. Hill, J. A. Nousek, A. A. Wells, A. T. Short, R. M. Ambrosi, G. Chincarini, O. Citterio, and G. Tagliaferri, "Swift x-ray telescope (XRT)," *Proc. SPIE* **4851**, pp. 1320–1325, 2003.
7. J. E. Hill, D. N. Burrows, J. A. Nousek, A. F. Abbey, R. M. Ambrosi, H. W. Bräuninger, W. Burkert, S. Campana, C. Cheruvu, G. Cusumano, M. J. Freyberg, G. D. Hartner, R. Klar, C. Mangels, A. Moretti, K. Mori, D. C. Morris, A. D. T. Short, G. Tagliaferri, D. J. Watson, P. Wood, and A. A. Wells, "Readout modes and automated operation of the Swift X-ray Telescope," *Proc. SPIE* **5165**, pp. 217–231, 2004.
8. G. Tagliaferri, A. Moretti, S. Campana, A. F. Abbey, R. M. Ambrosi, L. Angelini, A. P. Beardmore, H. W. Bräuninger, W. Burkert, D. N. Burrows, M. Capalbi, G. Chincarini, O. Citterio, G. Cusumano, M. J. Freyberg, P. Giommi, G. D. Hartner, J. E. Hill, K. Mori, D. C. Morris, K. Mukerjee, J. A. Nousek, J. P. Osborne, A. D. T. Short, F. Tamburelli, D. J. Watson, and A. A. Wells, "Swift XRT effective area measured at the Panter end-to-end tests," *Proc. SPIE* **5165**, pp. 241–250, 2004.
9. J. Osborne and et al., "The in-flight spectroscopic performance of the Swift XRT CCD Camera," *Proc. SPIE this volume*, 2005.
10. A. Moretti and et al., "Swift XRT Point Spread Function," *Proc. SPIE this volume*, 2005.
11. E. Massaro, M. Litterio, G. Cusumano, and T. Mineo, "The Crab pulsar in the INTEGRAL range," in *Exploring the gamma-ray universe. Proceedings of the Fourth INTEGRAL Workshop, 4-8 September 2000, Alicante, Spain. Editor: B. Battrick, Scientific editors: A. Gimenez, V. Reglero & C. Winkler. ESA SP-459, Noordwijk: ESA Publications Division*, pp. 229–233, 2001.

12. S. H. Pravdo, L. Angelini, and A. K. Harding, "X-Ray Spectral Evolution of the Crab Pulse," *The Astrophysical Journal* **491**, pp. 808–815, 1997.
13. A. Moretti and et al., "The simultanepus Swift-XRT/XMM-Newton Observation of the Afterglow of GRB 050326," *Astronomy and Astrophysics*, p. in preparation, 2005.
14. M. Kirsh and et al., "Crab: the standard X-ray candle with all (modern) X-ray satellites," *Proc. SPIE this volume* , 2005.